



## An innovative yttrium nanoparticles/PVA modified PSF membrane aiming at decontamination of arsenate

Yang Yu<sup>a,b</sup>, Ling Yu<sup>b,c</sup>, Chenghong Wang<sup>b,d</sup>, J. Paul Chen<sup>b,d,\*</sup>

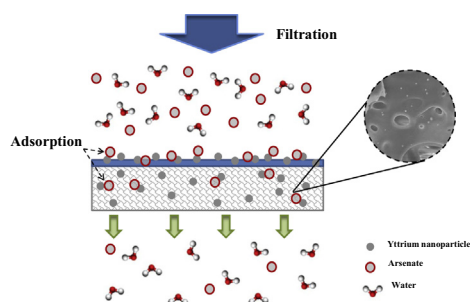
<sup>a</sup>Guangdong Key Laboratory of Environmental Pollution and Health, and School of Environment, Jinan University, Guangzhou 510632, China

<sup>b</sup>Department of Civil and Environmental Engineering, National University of Singapore, 10 Kent Ridge Crescent, Singapore 119260, Singapore

<sup>c</sup>School of Environmental Science and Engineering, Sun Yat-Sen University, Guangzhou 510006, China

<sup>d</sup>NUS Graduate School for Integrative Sciences and Engineering (NGS), National University of Singapore, Singapore 117456, Singapore

### GRAPHICAL ABSTRACT



### ARTICLE INFO

#### Article history:

Received 20 February 2018

Revised 27 May 2018

Accepted 3 June 2018

Available online 4 June 2018

#### Keywords:

YNPs/PVA modified PSF membrane

Arsenate

Adsorption

Filtration

Ligand exchange

### ABSTRACT

Arsenic contamination due to anthropogenic and natural activities has posted a great risk to humans through several pathways. As such, development of cost-effective technologies for arsenic decontamination is very important from both social and economic standpoints. In this paper, we are reporting a novel adsorptive yttrium nanoparticles (YNPs)/polyvinyl alcohol (PVA) modified polysulfone (PSF) membrane for the efficient treatment of arsenic. In the preparation of membrane, the porous PSF membrane fabricated with hydrophilic polyacrylic acid (PAA) polymer was coated by a PVA thin layer and then loaded with YNPs through an in-situ precipitation method using an ammonia vapor. We found that spherical YNPs were uniformly distributed onto the surface and within the matrix of membrane. The adsorption capacity as high as 35.56 mg-As/g was obtained at pH around 7. The membrane worked well across pH 4.0–8.0, with the best performance at pH 5.0. 90% of ultimate adsorption capacity was achieved in 2 h with the initial arsenic concentration of 10 mg/L and at the membrane dosage of 0.2 g/L. The kinetics data can be better fitted by the pseudo-second-order model. The Langmuir isotherm well described the adsorption isothermal data. The filtration studies with an initial arsenate concentration of 94.8  $\mu\text{g/L}$  showed that the treatment capacities of the composite membrane at pH 7.0 and 5.0 were 296 and 692  $\text{L/m}^2$ , respectively. The X-ray photoelectron spectroscopy (XPS) analysis suggested that ligand exchange between yttrium-hydroxyl groups and arsenate species may play as the main adsorption mechanism. Our study demonstrates that the membrane is a better material for arsenic decontamination than previously reported adsorptive membranes.

© 2018 Elsevier Inc. All rights reserved.

\* Corresponding author at: Department of Civil and Environmental Engineering, National University of Singapore, 10 Kent Ridge Crescent, Singapore 119260, Singapore.  
E-mail addresses: [paulchen@nus.edu.sg](mailto:paulchen@nus.edu.sg), [jpaulchen@gatech.edu](mailto:jpaulchen@gatech.edu) (J.P. Chen).

## 1. Introduction

High risk of arsenic contamination to human health affects many places in the world including China, India, Taiwan, and United States. This has triggered a great progress of arsenic treatment technologies in recent decades [1]. Compared to other technologies, adsorption is considered as the most favorable method for arsenic removal because of its ease in operation, great availability of adsorbents, and cost-effectiveness [2–6].

Several nano-sized metal based adsorbents have been developed for removal of aqueous arsenic, including nano zero-valent iron [7], nanocrystalline magnetite [8], nano-TiO<sub>2</sub> [9], and zirconium nanoparticles [10]. The adsorption performance of metal based adsorbents can be greatly improved whilst the adsorbents' particle size is reduced from millimeters to nanometers leading to much greater specific surface area and more rapid adsorption kinetics [8,11,12].

A highly active hydrated yttrium oxide (HYO) with the superior adsorption capacity has been reported recently [5]. The extremely high adsorption ability shows its promising potential towards practical application in remediation of arsenic-contaminated water. However, the wide application of nano-sized adsorbents is considerably constrained by the difficulty in separation of nanoparticles from treated water streams. Energy-consuming technologies such as centrifuge and filtration are therefore required to effectively isolate and then collect the spent nano-sized adsorbents.

In order to overcome the disadvantages in separation of nano-sized materials after use, adsorptive membranes (also called as functionalized or affinity membranes) have reportedly been fabricated by incorporating them in membrane matrix [4,13,14]. They can inherit the excellent adsorption performance of adsorptive nano-sized particles and meanwhile overcome separation challenge.

Owing to the presence of hydrophilic surface groups on metal based adsorbents (e.g., –OH group), the agglomeration of these particles is observed in the membrane casting solutions, such as PSF and poly(vinylidene fluoride) (PVDF) [13,15]. As a result, the particles in the membrane matrix are generally micrometer-scaled. The agglomeration can lead to the uneven distribution of active particles in the membrane matrix and potentially reduce their adsorption ability and kinetics. Therefore, it is rather important to develop better approaches to uniformly load the nano-sized adsorbents into the membrane matrix in the preparation of adsorptive membranes so that they can perform well in water treatment.

In this study, an in-situ precipitation method using ammonia vapor was reported for the first time to load YNPs onto the membrane surfaces and within the membrane matrix. In order to better immobilize and distribute YNPs, PVA was used for surface modification of PSF membrane, as the positively charged yttrium ions may form the complexes with the hydroxyl groups on PVA polymer via the Lewis acid-base pair [16]. Herein, the prepared membrane was applied for the removal of arsenate from water. The membrane properties including membrane morphology, water flux, total porosity and point of zero charge (PZC) were examined. The adsorption performance of the membrane towards arsenate was investigated in both batch adsorption and filtration modes. XPS as well as Fourier transform infrared spectroscopy (FTIR) were employed for the mechanism study.

## 2. Materials and methods

### 2.1. Materials

Unless otherwise stated, all chemicals were of analytical grade and used directly from purchase without further purification.

Yttrium(III) nitrate hexahydrate (Y(NO<sub>3</sub>)<sub>3</sub>·6H<sub>2</sub>O), sodium fluoride (NaF), sodium dihydrogen phosphate (NaH<sub>2</sub>PO<sub>4</sub>), sodium bicarbonate (NaHCO<sub>3</sub>), sodium sulphate (Na<sub>2</sub>SO<sub>4</sub>), hydrogen chloride (HCl), humic acid (HA) (sodium salt), dimethylformamide (DMF), polysulfone (26,000 Da), glutaraldehyde aqueous solution (GLA, Grade II, 25%), polyacrylic acid (PAA, ~450,000 Da) and polyethylene glycol (PEG, MW = 35,000, 100,000, 200,000, 300,000, 400,000 and 600,000 Da) were purchased from the Sigma-Aldrich (Singapore). Polyvinyl alcohol (PVA, 72,000 Da) and sodium hydrogen arsenate heptahydrate (Na<sub>2</sub>HAsO<sub>4</sub>·7H<sub>2</sub>O) were purchased from the Fluka (Switzerland). Nitric acid (HNO<sub>3</sub>) and sodium hydroxide (NaOH) were obtained from the Merck (Germany).

The preparation of As(V) stock solution was through dissolving the specific amount of Na<sub>2</sub>HAsO<sub>4</sub>·7H<sub>2</sub>O in deionized (DI) water. The respective working solutions of As(V) were obtained through the dilution of this stock solution using DI water.

### 2.2. Fabrication of composite membrane

The preparation of porous PSF membrane was as follows: (1) The PSF and PAA were respectively dissolved in DMF under stirring at 90 °C; (2) The polymer solutions were mixed together in polymer weight ratio of 90:10 and stirred for at least 3 h to obtain a uniform solution; (3) After being degassed overnight, the mixed polymer solution was homogeneously casted on glass plates and then immersed in DI water; (4) The formed membrane with the thickness of 150 μm was kept in DI water for more than 48 h to remove the residual solvents.

The coating of PVA layer onto the PSF membrane substrate was carried out as follows: (1) The solution of PVA (0.5 wt%) was prepared by dissolving 0.5-g PVA in 100-mL DI water under stirring at 90 °C; (2) The PSF substrate was immersed in the prepared PVA solution for 1 h before drying; (3) After drying, the substrate was then immersed and soaked in a mixture of GLA (4 wt%) and HCl (10 mM) for 30 min to trigger the cross-linking reaction; (4) The substrate was rinsed and washed using DI water to get rid of residual PVA and GLA; (5) Finally, the PVA coated PSF membrane was dried in air and stored.

The loading of yttrium nanoparticles to the PVA coated PSF membrane was conducted as follows: (1) The solution of 0.1 M yttrium nitrate was prepared through the dissolution of Y(NO<sub>3</sub>)<sub>3</sub>·6H<sub>2</sub>O into absolute ethanol; (2) The composite membrane was immersed into yttrium/ethanol solution at ambient temperature for 2 h; (3) The resultant membrane containing yttrium ions was treated by ammonia vapor overnight; compared to immersing the membrane into ammonium hydroxide or other basic solutions, the treatment of ammonia vapor can ensure most of the bonding yttrium ions to be in-situ precipitated on the membrane; (4) The membrane was finally washed with DI water in order to fully remove the unreacted yttrium and ammonia before drying in air.

### 2.3. Membrane characterization

The surface morphology of membranes was studied using a field emission scanning electron microscope (FESEM, JSM-6701F, JEOL, Japan). To prepare the samples for imaging analysis of the cross-section, the membranes were first immersed in the liquid nitrogen and cut to smaller pieces. Prior to the test, the membrane samples were coated with platinum for sufficient electric conductivity. Moreover, the surface elemental distribution of membranes was investigated by the equipped energy dispersive X-ray spectrophotometer (EDX, JEOL JED 2300).

The total porosity of the membrane was measured by the gravimetric method. The membrane weight was measured, and was successively immersed in ethanol and DI water for 10 min. It was then kept in DI water overnight. Afterwards, delicate task wipers

were used to remove the water on the surface of membrane, and the wet weight of the membrane was recorded. The same procedure was repeated for three times. The total porosity can be calculated as follows. The averaged value is reported in this paper; the experimental error is within 5%.

$$\text{Total porosity}(P) = \frac{(m_w - m_d)}{\rho_{\text{water}} \times V} \quad (1)$$

where  $m_w$  and  $m_d$  (g) are the weight of the wet and dry membranes, respectively;  $\rho_{\text{water}}$  (1 g/cm<sup>3</sup>) is the water density at 25 °C; and  $V$  (cm<sup>3</sup>) is the volume of the dry membrane.

The pure water flux (PWF) of the membrane was tested by using the Merck Millipore stirred cell module (8050, USA) under the operation pressure of 2 bar. The effective area of the membrane (through measurement) was 12.56 cm<sup>2</sup> in the filtration study. The PWF can be determined by the following equation:

$$J_w = \frac{Q}{S \cdot t \cdot p} \quad (2)$$

where  $J_w$  (L/m<sup>2</sup>·h·bar) is the pure water flux,  $Q$  (L) is the volume of the permeated water,  $t$  (h) is the time interval,  $p$  (bar) is the operation pressure, and  $S$  (m<sup>2</sup>) is the effective membrane surface area.

The molecular weight cut-off (MWCO) of the membrane was measured by filtrating the PEG solutions (with different molecular-weights) with the initial concentration of 100 mg/L. The MWCO refers to the lowest molecular weight of PEG, of which 90% can be efficiently rejected by the membrane. The filtration tests were carried out under an operation pressure of 2 bar. The rejection rate can be calculated by the following equation:

$$R = \left(1 - \frac{C_p}{C_f}\right) \times 100\% \quad (3)$$

where  $R$  (%) is the PEG rejection rate, and  $C_p$  and  $C_f$  (mg/L) are the PEG concentrations of permeation and feed solutions. Specifically, the PEG concentrations were measured using a total organic carbon analyzer (TOC-4100, Shimadzu, Japan).

The surface functional groups on the membrane were studied by using the FTIR (Shimadzu, Japan) in the attenuated total reflection (ATR) mode with a germanium crystal. Every scan was taken across a wavenumber range of 500–4000 cm<sup>-1</sup> at the ambient temperature.

The PZC was determined by a previously reported method [17]. The membrane was suspended in a NaNO<sub>3</sub> solution of 0.01-M with a volume of 50-mL for 24 h. The pH of each suspension was respectively adjusted to different values ranging from 3 to 10 by adding NaOH or HNO<sub>3</sub>. After agitating the suspensions for 60 min to establish equilibrium, the exact pH values were recorded and considered as the initial pH. After that, NaNO<sub>3</sub> was added at a concentration of 0.45 M. After stirring for another 3 h, the final pH value of each suspension can be recorded. The PZC was determined in the plot of  $\Delta\text{pH}$  (final pH - initial pH) vs. final pH, where the  $\Delta\text{pH}$  equals to zero.

#### 2.4. Batch adsorption study

An adsorption kinetics study was carried out to obtain the adsorption rate so that the adsorption equilibrium time was obtained. The batch equilibrium experiments on the adsorption were designed to find out effects of pH and competitive factors on the adsorption performance, and adsorption capacity through the adsorption isotherm study. With such basic information, one can start a preliminary design of treatment system as well as better understand the adsorption process.

In the adsorption kinetics experiment, 0.2-g membrane was added into a 1-L arsenate solution ( $C_0 = 10$  mg-As/L). Throughout

the adsorption process, the pH of solution was constantly monitored and manually maintained at 7.0. The samples were taken at different time intervals to measure the arsenate concentrations by an inductively coupled plasma optical emission spectrometer (ICP-OES, PerkinElmer Optima 3000).

In the pH effect experiment, a number of 50-mL arsenate solutions (10 mg-As/L) were respectively prepared at different pH (3–10). The pH of solutions was fixed during the adsorption via the addition of HNO<sub>3</sub> or NaOH. Then, 0.2-g membrane was trimmed out and added into each arsenate solution, which was constantly shaken on a rotary shaker. After 24 h, aliquots of solution samples were taken for the measurement of arsenic concentration by the ICP-OES.

In the experiment of adsorption isotherm, 0.02-g membrane was added in several 100-mL arsenate solutions at different concentrations (1–60 mg-As/L). Throughout the study, the pH of solutions was constantly monitored and manually maintained at 7.0 by adding HNO<sub>3</sub> or NaOH solutions. Other experimental procedures were the same as those in the pH effect study.

In the experiment of co-existing substance effect, NaH<sub>2</sub>PO<sub>4</sub>, Na<sub>2</sub>SO<sub>4</sub>, NaF, NaHCO<sub>3</sub> and HA as representative substances were respectively added into 10 mg-As/L arsenate solutions. The membrane dosage (m) was 0.2 g/L. The solution pH was constantly monitored and manually maintained at 7.0 by adding NaOH or HNO<sub>3</sub> during the adsorption process. Other procedures were the same as those in the experiment of pH effect.

#### 2.5. Filtration study

The filtration study was conducted in a stirred cell module equipped with an 800-mL feed tank (Model 8050, Merck Millipore). To start with, a small portion of the membrane with an effective area of 12.56 cm<sup>2</sup> was trimmed out for the use in arsenate rejection. The operation pressure of 2 bar was introduced by applying a compressed nitrogen gas on the water. The concentration of As(V) in the feed solution of 94.8 μg/L and the influent pH around 7.0 were controlled. Aliquots of the effluents that flew out at different time intervals were collected to measure the respective arsenate concentrations.

To regenerate the saturated membrane, the spent membrane after the filtration was immersed in 0.01 M NaOH for 12 h. Afterwards, the regenerated membrane was washed by the DI water thoroughly and then dried before being used into next round of application. Other procedures were the same as the filtration study.

#### 2.6. X-ray photoelectron spectroscopy

The XPS studies were carried out using a spectroscope (Kratos XPS system-Axis His-165 Ultra, Shimadzu, Japan). The instrument provides a monochromatized AlK $\alpha$  X-ray source (1486.71 eV), which works at a condition of 15 kV, 10 mA and 150 W. Within the analytical chamber, a base pressure of  $3 \times 10^{-8}$  Torr is maintained. Herein, we collected the information in terms of the binding energy.

A non-linear least-square curve fitting program called XPSPEAK41 Software was then used for the analysis of the collected data. To calibrate, the graphitic carbon with a binding energy of 284.8 eV was selected as the reference to correct the carbon signal. This is for the sake of compensating charging effect. Further to that, the respective XPS spectra with respect to the elements of yttrium, oxygen and arsenic were deconvoluted based on the Gaussian (20%)-Lorentzian (80%) mixed function after the subtraction of a linear background. The detection limits of XPS spectra on the measurement of the element composition are in the range of parts of thousand (1000 ppm) [18].

### 3. Results and discussion

#### 3.1. Characterizations of composite membrane

##### 3.1.1. Morphology and elemental distribution study

The morphology imaging towards the surface and cross-section of membranes can be found in Fig. 1. The pristine PSF membrane has a dense surface layer and porous sponge-like matrix as shown in Figs. 1a and b.

After adding the hydrophilic polymer PAA to the membrane casting solution, numerous large pores emerge on the membrane surface. Many figure-like cavities and macrovoids are formed on the cross-section of the membrane as shown in Figs. 1c and d. The PAA polymer works similarly as the other pore-forming additives (e.g., polyvinyl pyrrolidone (PVP) and PEG). It accelerates the diffusion rate of the solvent (DMF)/non-solvent (DI water) during

phase inversion, leading to the formation of big cavities and macrovoids [19–21]. Moreover, the immobilization of hydrophilic PAA into the inert PSF matrix can reportedly generate cation exchange capacity, resulting in higher rejection of lead, cadmium and chromium [22]. This would be beneficial for the attachment of yttrium cations on the porous PSF membrane during the modification process.

Fig. 1e clearly shows that large pores on the PSF membrane surface are covered by the PVA layer. The surface pore size and water flux of the membrane can therefore be adjusted by the thickness of PVA thin layer. Moreover, a large number of spherical nanoparticles uniformly distribute on the surface of YNPs/PVA modified PSF membrane after further being treated by yttrium solution and ammonia vapor. From the high-resolution FESEM image of the insert of Fig. 1f, the uniformly distributed yttrium nanoparticles can also be observed in the matrix of YNPs/PVA modified

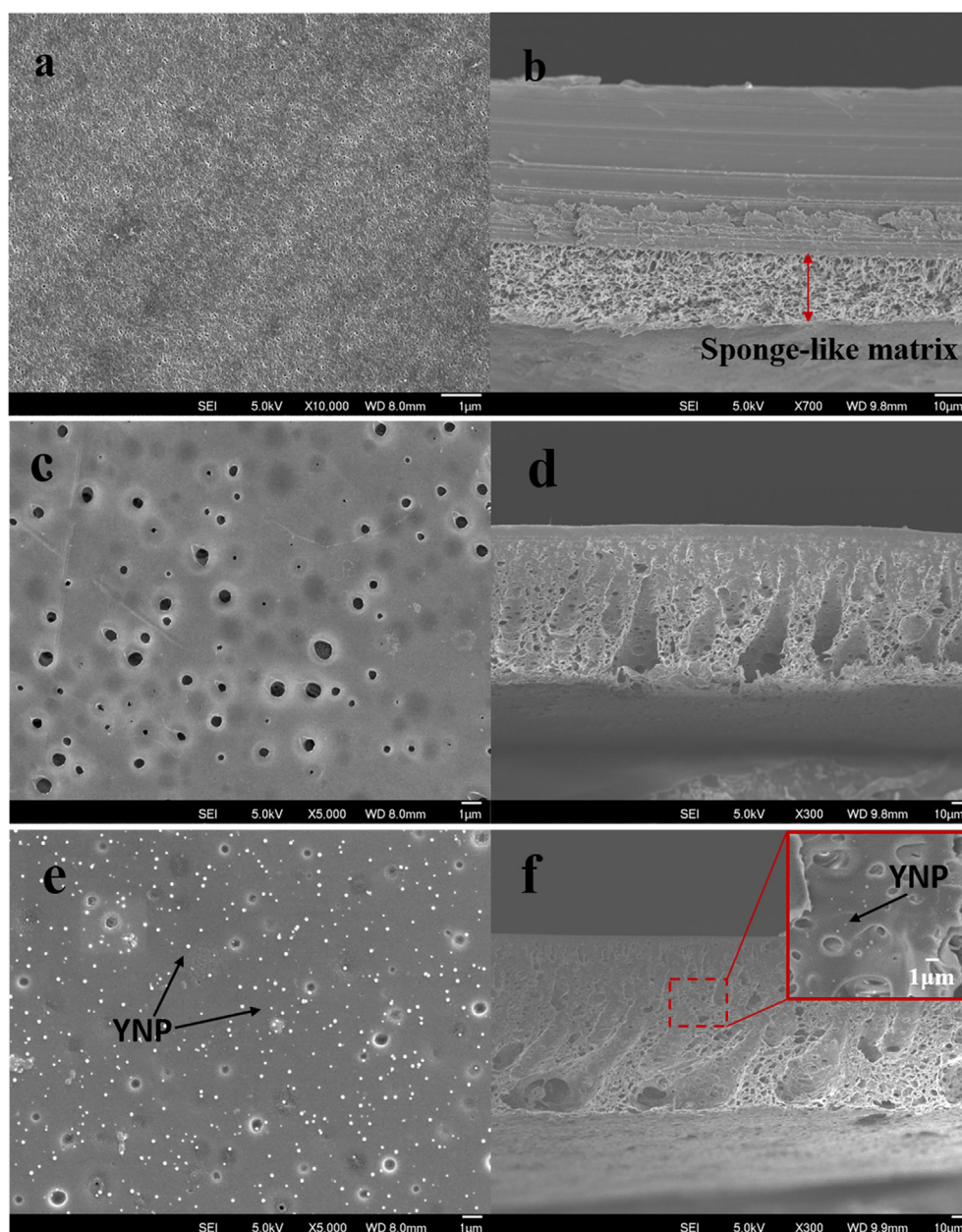


**Fig. 1.** FESEM imaging on membranes: (a) surface and (b) cross-section morphologies with respect to pristine PSF membrane; (c) surface and (d) cross-section morphologies with respect to porous PSF membrane (PAA as a pore-forming additive); (e) surface and (f) cross-section morphologies with respect to YNPs/PVA modified PSF membrane.

PSF membrane. The element distribution of YNPs/PVA modified PSF membrane surface shown in Fig. S1 confirms the presence of yttrium nanoparticles on the membrane.

### 3.1.2. Physical characteristics of membranes

As illustrated in Table 1, the porosity of the PSF membrane increases from 41.0 to 67.9% after adding PAA to the casting solution. This is consistent with the observation from the FESEM imaging. The porosity of membrane decreases to 62.6% after the coating

**Table 1**  
Physical characteristics of membranes.

Membrane	Porosity (%)	Flux (L/h·m <sup>2</sup> ·bar)	MWCO (KDa) <sup>a</sup>
Pristine PSF	41.0	–	–
Porous PSF <sup>b</sup>	67.9	286.6	550
PVA modified PSF	62.6	66.9	250
YNPs/PVA modified PSF	58.4	97.9	150

– Refers to the value that cannot be measured due to the limit of operation pressure.

<sup>a</sup> Represents the lowest molecular weight of PEG of which 90% can be rejected by the membrane.

<sup>b</sup> Porous PSF refers to the PSF membrane after adding PAA as a pore-forming additive.

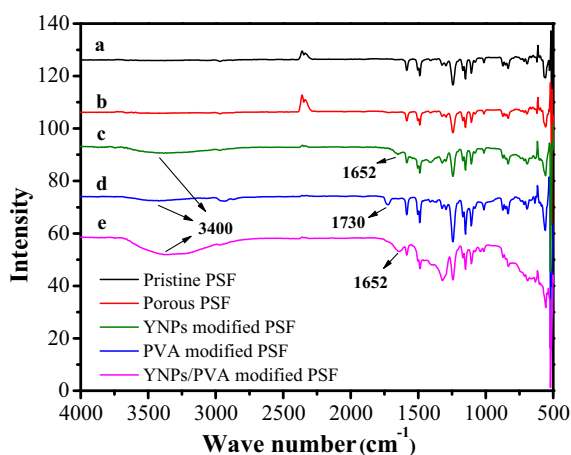


**Fig. 2.** FTIR spectra of membranes: (a) pristine PSF membrane; (b) porous PSF membrane; (c) YNPs modified PSF membrane; (d) PVA modified PSF membrane; (e) YNPs/PVA modified PSF membrane.

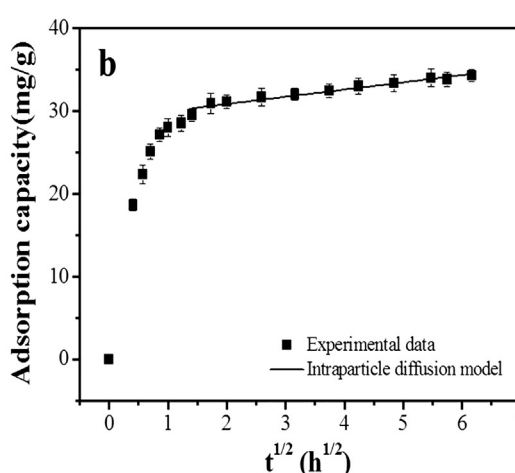
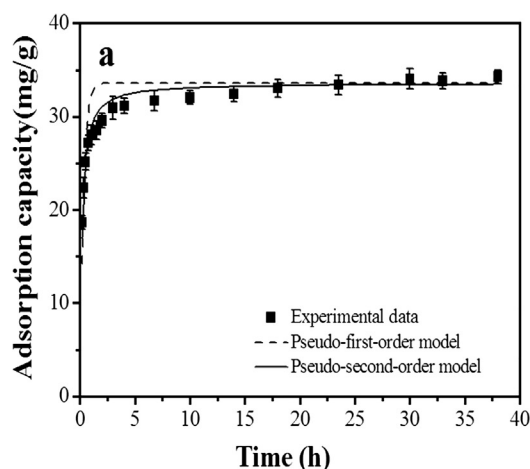


**Fig. 3.** Arsenate adsorption kinetics of YNPs/PVA modified PSF membrane: (a) experimental data and modeling results from the pseudo-first-order and pseudo-second-order models; (b) intraparticle diffusion model. Experimental conditions: [As]<sub>0</sub> = 10 mg-As/L, m = 0.2 g/L, pH = 7.0, T = 25 °C.

of PVA layer and further drops to 58.4% after the loading of YNPs on the membrane. The rejection of different molecular-weight PEG by membranes is shown in Fig. S2 with the corresponding MWCO values given in Table 2. Similar to the membrane porosity, the MWCO decreases from 550 to 250 KDa after the PVA modification and further drops to 150 KDa after loading the YNPs. However, a significant increase in water flux is found for the YNPs/PVA modified PSF membrane in comparison to the PVA modified PSF membrane. Similar to other studies, the incorporation of metal oxide nanoparticles in the membrane may lead to a significant increase in membrane hydrophilicity and consequently facilitate the water permeation [13–15].

### 3.1.3. FTIR study

The FTIR spectra of pristine PSF, porous PSF, YNPs modified PSF, PVA modified PSF and YNPs/PVA modified PSF membranes were all studied to identify the change of chemical structures of the membranes after the modification steps. As shown in Figs. 2a and b, no additional new peak is found in the spectrum of the porous PSF membrane compared to that of the pristine PSF membrane, indicating that water-soluble PAA polymer may mainly contribute to the increase in the membrane porosity.

After loading YNPs on the porous PSF membrane, two new peaks at 3400 and 1652 cm<sup>-1</sup> appear in Fig. 2c, which can respectively be ascribed to the O-H stretching vibration of the adsorbed water molecule [23] and surface hydroxyl groups (–OH groups) [24]. This confirms the presence of hydroxyl groups on the yttrium nanoparticles. Moreover, the appearance of the peak at 1730 cm<sup>-1</sup> (Fig. 2d) can be attributed to the presence of the C=O groups, resulting from the occurrence of non-complete cross-linking reaction of PVA with GLA. It is worthwhile to note in Fig. 2e that the strength of the peak at 3400 cm<sup>-1</sup> significantly increases as the co-existence of the PVA and YNPs on the membrane surface, while the characteristic peaks assigned to –OH and C=O bands are found to be overlapped.

## 3.2. Batch adsorption study

### 3.2.1. Adsorption kinetics

As illustrated in Fig. 3a, the membrane demonstrates a rapid uptake towards the As(V) species; within the first 30 min, more than 74% of the ultimate adsorption capacity (25.14 mg-As/g) can be accomplished. After the initial stage 30 min, the uptake slows down and reaches the equilibrium in 10 h.

A comparison of adsorption rate and capacity of different adsorptive membranes is shown in Table S1 (in terms of “adsorption capacity in 30 min” and “max. adsorption capacity”). The YNPs/PVA modified PSF membrane outperforms others as it has larger values in both parameters. This indicates its great potential for treatment of arsenic-contaminating water.

The adsorption kinetics of YNPs modified PSF and PVA modified PSF membranes was studied. As shown in Fig. S3, the ultimate adsorption capacities of YNPs modified PSF and PVA modified PSF membranes are 15.76 and 1.56 mg-As/g, respectively; this suggests that YNPs loading is crucial for the enhancement of the arsenic adsorption onto the membrane and the PVA layer can provide more binding sites for yttrium ions.

The experimental data of adsorption kinetics was analyzed by the pseudo-first-order and pseudo-second-order equations; their mathematical equations are as below [25,26]:

$$q_t = q_e(1 - e^{-K_1 t}) \quad (4)$$

$$q_t = \frac{K_2 q_e^2 t}{1 + K_2 q_e t} \quad (5)$$

where  $q_e$  and  $q_t$  (mg-As/g) are the adsorption capacities at equilibrium and time  $t$  (h), respectively;  $K_1$  ( $\text{h}^{-1}$ ) and  $K_2$  ( $\text{g} \cdot \text{mg}^{-1} \cdot \text{h}^{-1}$ ) are the equilibrium constants of the pseudo-first-order and pseudo-second-order models, respectively.

As listed in Table S2, the pseudo-second-order model has a higher correlation coefficient value ( $r^2$ ), indicating that it better describes the uptake profile than the pseudo-first-order model. Furthermore, this indicates that the adsorption is controlled by a chemisorption process [27].

In addition, the non-linear chi-square test ( $\chi^2$ ) given below was applied to validate an appropriate kinetics model.

$$\chi^2 = \sum \frac{(q_t - q_{t,m})^2}{q_{t,m}} \quad (6)$$

where  $q_t$  is the adsorption capacity determined in experiment (mg-As/g), and  $q_{t,m}$  is the adsorption capacity calculated using the equations (mg-As/g).

As shown in Table S2, the value of  $\chi^2$  from the pseudo-second-order kinetics model is much smaller than that from the pseudo-first-order model; this suggests that the pseudo-second-order kinetics model is more suitable for simulating the experimental data.

Compared to our previous study on the removal of As(V) by hydrated yttrium oxide particles, the adsorption rate constant ( $K_1$ ) from the pseudo-first-order model with respect to the composite membrane is 10 times higher than that of hydrated yttrium oxide particles [5]. The rapid adsorption of As(V) on the membrane may be due to the uniform distribution of YNPs on both surface and matrix of the membrane.

The rate-limiting step of the adsorption process was determined using the intraparticle diffusion model with an equation as follows [28]:

$$q_t = K_{id} t^{1/2} + \alpha \quad (7)$$

where  $K_{id}$  ( $(\text{mg/g})/\text{h}^{1/2}$ ) is the intraparticle diffusion rate constant;  $\alpha$  (mg-As/g) is a constant that reflects the significance of boundary layer or external mass transfer effect. The larger  $\alpha$  value means the greater contribution of the surface adsorption to the rate-controlling step.

As shown in Fig. 3b, the adsorption has a two-phase profile: an initial smooth curve followed by a linear portion. The first adsorption step shall be governed by the boundary layer effect till the adsorbed amount of As(V) reaches about 85% of ultimate

adsorption capacity. Afterwards, the adsorption process is controlled by the intraparticle diffusion.

### 3.2.2. pH effect

Chemisorption plays the most important role in adsorption of metals and organic compounds in aqueous solutions. In addition, the electrostatic interaction between the adsorptive materials and the As(V) affects the performance to some extent, since the net surface charge of the material and the speciation form of arsenic are pH-dependent [29].

The surface charge of the YNPs/PVA modified PSF membrane and species distribution of As(V) with regards to the solution pH are respectively shown in Figs. S4a and b. It is found that the PZC value of the composite membrane is approximately 7.2. When the solution pH is above its PZC value, the membrane is negatively charged. On the contrary, it is positively charged at  $\text{pH} < 7.2$ . As shown in Fig. S3b, the dominant species of As(V) are  $\text{H}_2\text{AsO}_4^-$  and  $\text{HAsO}_4^{2-}$  in pH of 3–7 and 7–10, respectively.

Two sets of experiments were conducted to examine the influence of solution pH on the As(V) uptake: with pH controlling at fixed values and without pH controlling during the adsorption. The results are given in Fig. 4.

Under the pH controlling condition, the adsorption capacity of As(V) increases from pH 3.0 to 5.0. It reaches the optimal value of 40.75 mg-As/g at pH 5.0.

Since the yttrium nanoparticles are formed by an in-situ precipitation method using ammonia vapor, they become less stable at pH 3.0, which results in the obviously lower As(V) uptake. In addition, at lower pH (e.g., pH 3), the arsenic is in the form of  $\text{H}_3\text{AsO}_4$  as shown in Fig. S4b. As it does not carry any negative charge, no uptake of arsenic can happen according to the general rules of chemical adsorption and ion exchange.

When the pH is shifted from 3 to 5, more negatively charged arsenic species become available ( $\text{H}_2\text{AsO}_4^-$ ). The protonated hydroxyl group on the membrane ( $-\text{OH}_2^+$ ) at  $\text{pH} < 7.2$  can better adsorb the negatively charged arsenic species [30]. In addition, the electrostatic attraction between the positively charged membrane and  $\text{H}_2\text{AsO}_4^-$  can further facilitate the uptake of As(V).

As the solution pH is further increased from 5 to 10, the uptake slowly becomes retarded due to several reasons, namely, 1. the protonated hydroxyl group becomes less as pH is increased; 2. the electrostatic repulsion increases between the negatively

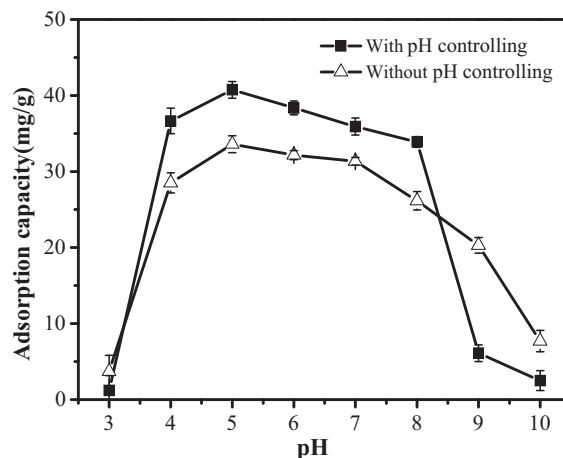


Fig. 4. Effects of solution pH on arsenate adsorption by YNPs/PVA modified PSF membrane: adsorption capacity under different pH with/without pH controlling. Experimental conditions:  $[\text{As}]_0 = 10$  mg-As/L;  $m = 0.2$  g/L;  $t = 24$  h;  $T = 25$  °C. Noted: The pH shown for the not-pH controlled cases is the initial pH.

charged membrane (at  $\text{pH} > \text{PZC}$ ) and  $\text{HAsO}_4^{2-}$ ; 3. the competition between hydroxide ions in the solution and arsenic species towards the active sites on the composite membrane becomes intense [31].

The similar trend of the adsorption capacity with regards to the solution pH is observed under the non-controlled pH condition. The membrane shows better performances at the initial pH of 3, 9 and 10 than those under the controlled pH condition. In addition, we observed slight increase in the solution pH after the adsorption. This is due to the effect of hydroxyl group on the uptake of arsenic, which is discussed in the XPS study.

### 3.2.3. Adsorption isotherm

The experimental isotherm curve at pH 7.0 together with the fitting by the Langmuir and the Freundlich equations is given in Fig. 5. The relevant parameters and their values obtained from both Langmuir and Freundlich equations are shown in Table S3. According to the correlation coefficients ( $r^2$ ), the Langmuir equation describes the experimental data better than the Freundlich equation. This suggests a monolayer adsorption process taking place during the As(V) uptake. Moreover, the maximum adsorption capacity given by the Langmuir equation is 35.56 mg-As/g at pH 7.0. Overall, the adsorption capacity of YNPs/PVA modified PSF membrane towards As(V) is mainly limited by the loading of YNPs.

### 3.2.4. Effect of co-existing substances

To understand the selectivity of the composite membrane towards arsenate species, we studied the effects from most commonly existing anions on the arsenic uptake. It is common that several negatively charged species well exist in natural waters and may compete with anionic arsenate species for the active sites during the water treatment. The important anions include carbonate, sulfate, fluoride, phosphate and natural organic matters (NOMs). The humic acid (anionic, and in a form of sodium salt) is chosen as the representative of the NOMs in this study.

As shown in Fig. S5, the influence of co-existing substances on the adsorption follows by a descending order of: phosphate > fluoride > sulphate > bicarbonate > HA. As the concentration of competing anion is increased, one can see that the negative effect becomes more severe.

The presence of 10-mM phosphate or fluoride in solution has the negative effects on the As(V) uptake; the adsorption decreases from 35.2 to 7.3 and to 17.4 mg-As/g in the presence of phosphate and fluoride, respectively. It should be noted that the typical concentrations of phosphate and fluoride in natural waters are generally in a range of 0–5 mg/L (<0.15 mM) and 0.01–3 mg/L

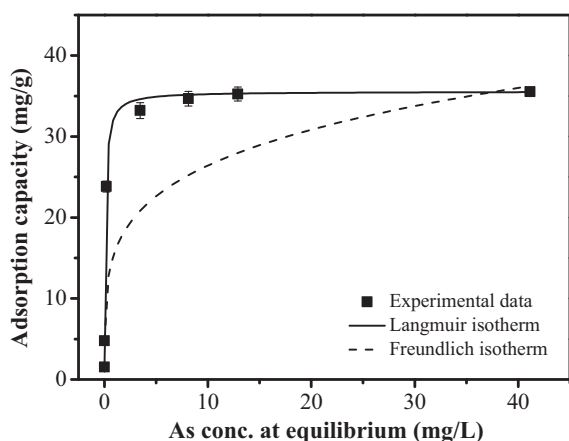


Fig. 5. Arsenate adsorption isotherm of YNPs/PVA modified PSF membrane. Experimental conditions:  $m = 0.2 \text{ g/L}$ ;  $\text{pH} = 7.0$ ;  $t = 24 \text{ h}$ ;  $T = 25 \text{ }^\circ\text{C}$ .

(0.5  $\mu\text{M}$ –0.16 mM), respectively, much lower than 10 mM used in our study [32,33]. Therefore, the influence of their presence on the performance in the practical applications would be less significant. Similar to other reported yttrium-based adsorbents, the strong competitive effect from phosphate or fluoride is due to the high affinity of two anions for the membrane.

Compared to the co-existing phosphate and fluoride anions, the presence of carbonate, sulfate and HA in water seems to have less negative effect on the adsorption. Typically, the concentrations of bicarbonate and sulfate are less than 1 and 0.5 mM, respectively. As such, the uptake capacity for arsenic can be reduced by 20–30% when carbonate or sulfate is present in the water. The less negative effect of 10–15% from the NOMs can be seen from the figure.

These findings on the other hands imply that the membrane can work well for removal of these anionic substances. A zirconium based nanoparticle developed by our lab showed that its removal for arsenic was negatively affected by the presence of fluoride and other anionic substances [10]. The further study on the same particle demonstrated that it was able to effectively remove fluoride from water solutions [34]. Based on the present study, we foresee that the membrane can work well to remove such anions as fluoride and phosphate ions, making it to be multi-functional for water treatment.

### 3.3. Filtration study

Both virgin and regenerated YNPs/PVA modified PSF membranes were tested for the As(V) removal in a dead-end filtration mode. The simulated arsenic-contaminated water feed with an initial concentration of 94.8  $\mu\text{g/L}$  was prepared by adding As(V) into DI water. The Maximum Contaminant Level (MCL) in drinking water is set by the US EPA and WHO for a list of contaminants. The MCL for the arsenic has been set at 10 ppb (10  $\mu\text{g/L}$ ) since early 2006.

As shown in Fig. 6, the virgin membrane can effectively treat more than 4200 (about 869 mL) and 1800 bed volumes (about 372 mL) of arsenic-contaminated water to ensure the arsenic concentration of effluents less than the MCL (10  $\mu\text{g/L}$ ) at pH 5.0 and 7.0, respectively [35]. According to the effective volume and area of the membrane, the treatment capacity of virgin composite membrane can be calculated as 692  $\text{L/m}^2$  at pH 5.0 and 296  $\text{L/m}^2$  at pH 7.0, respectively.

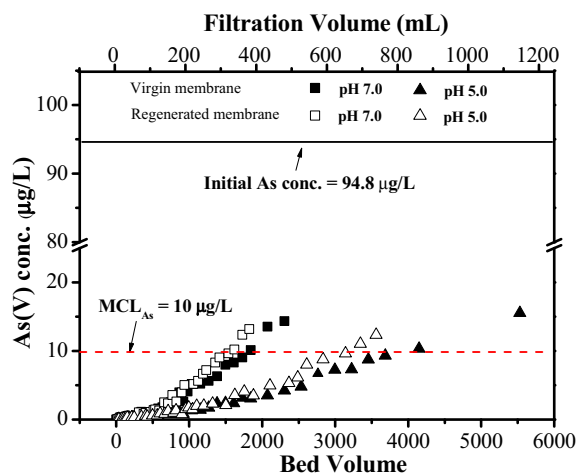


Fig. 6. Filtration study of As(V) removal by both the virgin and regenerated YNPs/PVA modified PSF membranes. Experimental condition:  $[\text{As}]_0 = 94.8 \text{ } \mu\text{g/L}$ , operation pressure = 2 bar, membrane volume = 0.207  $\text{cm}^3$ , membrane effective area = 12.56  $\text{cm}^2$ ,  $T = 25 \text{ }^\circ\text{C}$ .

In regards to the regenerated membrane, a slight reduction of treatment ability at pH 5.0 and 7.0 can be observed when repeating the same filtration procedure. This indicates that the composite membrane has a decent regeneration ability and can be reused through a simple regeneration process.

In addition, we observed slight increase in the pH in effluent solution during the filtration. This is due to the interaction between hydroxyl group on the membrane and arsenic.

### 3.4. Mechanism study

As shown in Fig. 7, the characteristic peaks of yttrium including Y 4p, Y 3d, and Y 3p can be found in the wide scan XPS spectrum of the virgin YNPs/PVA modified PSF membrane. Besides, two characteristic peaks referring to arsenic can be identified after the adsorption, namely As 3d and As LMM. The finding confirms that As(V) is successfully adsorbed on the membrane. In addition, the presence of S 2s peak in both virgin and As-loaded composite membranes should be attributed to the PSF polymer.

As shown in Fig. S6, the high-resolution scan spectrum of Y 3d with respect to the virgin YNPs/PVA modified PSF membrane can be decomposed into two component peaks with the binding energies of 158.3 and 160.3 eV, respectively. After the adsorption, the binding energies of these two component peaks shift to 158.4 and 160.4 eV respectively, due to the binding of more electronegative arsenate species on yttrium atoms.

In order to further explore the adsorption mechanism, the high-resolution scan XPS spectra of O 1s with respect to the virgin and As-loaded composite membranes were analyzed and the results are shown in Fig. 8. Specifically, we can decompose the O 1s spectrum of the virgin membrane into four component peaks, of which the peaks at the binding energies of 530.80, 531.60, 532.47, 533.17 eV can be assigned to C–OH, C–O/C=O, Y–OH and S=O respectively. Among them, C–OH, C–O/C=O and S=O shall stem from the polymers (i.e., PSF, PAA and PVA), while Y–OH bond is assigned to the hydroxyl group bonded to yttrium atoms. After the adsorption, a new component peak can be identified as the As–O bond [13].

As illustrated in Table S4, the relative content of As–O bond increases to 5.66% after the adsorption. Meanwhile, the relative content of Y–OH significantly decreases from 30.97% to 11.64%. This indicates that the exchange between hydroxyl groups and As(V) may be the possible mechanism for the arsenic uptake.

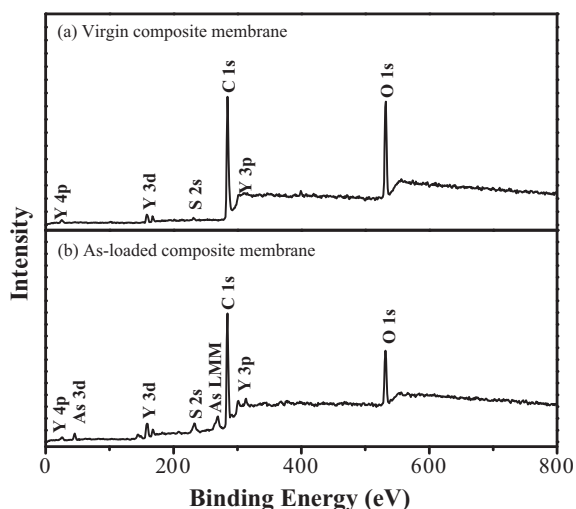


Fig. 7. XPS wide scan spectra with respect to YNPs/PVA modified PSF membranes before and after the adsorption.

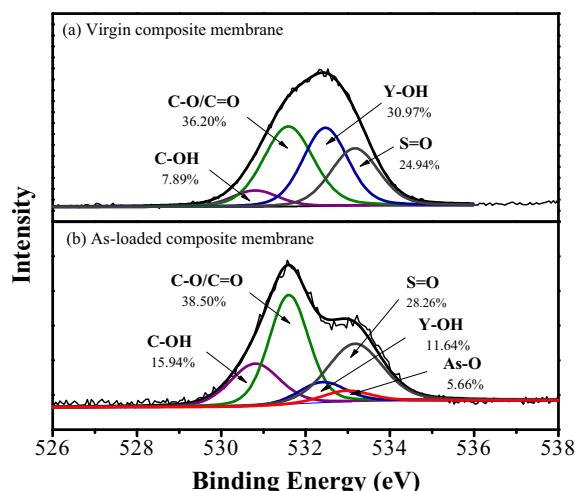


Fig. 8. XPS spectra of O 1s of YNPs/PVA modified PSF membranes: (a) virgin composite membrane; (b) As-loaded composite membrane.

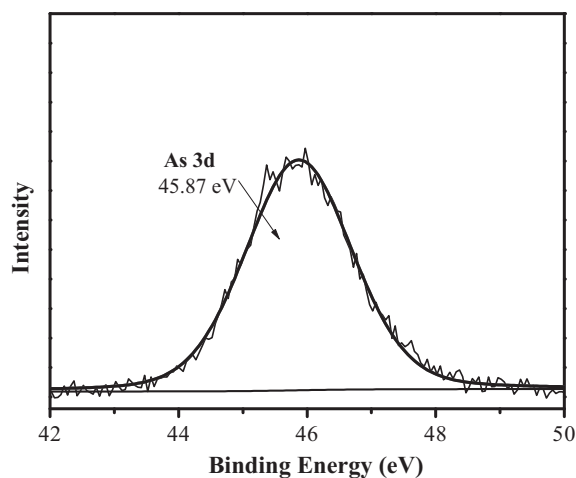


Fig. 9. As 3d XPS spectrum with respect to As-loaded YNPs/PVA modified PSF membrane.

The As 3d scan spectrum with respect to the post-adsorption YNPs/PVA modified PSF membrane is shown in Fig. 9. The characteristic peak appearing at 45.87 eV can be attributed to As(V) [6,36]. This indicates that there is no reduction of As(V) & As(III) chemical happening.

## 4. Conclusions

In the present study, we have successfully developed and optimized a novel YNPs/PVA modified PSF membrane for the adsorptive removal of arsenate from water. The yttrium nanoparticles were uniformly loaded on the membrane surface and matrix through the adsorption in-situ precipitation method using ammonia vapor. The usage of hydrophilic polymers PAA and PVA in the membrane preparation process can significantly affect the total porosity as well as the surface pore size of the membrane. The membrane can effectively remove arsenate from water across a wide pH range of 4.0–8.0. The adsorption kinetics data can be well fitted by the pseudo-second-order models. Owing to the uniform distribution of spherical yttrium nanoparticles, about 74% of ultimate adsorption capacity could be achieved in the first 30 min. The isotherm study suggested that the maximum adsorption

capacity of the membrane was 35.56 mg-As/g under neutral pH. The membrane with an area of 12.56 cm<sup>2</sup> was able to treat the arsenic-contaminated water at an initial concentration of 94.8 µg/L and with a 4200 bed volume (869 mL) to meet the regulation of arsenic in drinking water. The XPS study revealed that ligand exchange between hydroxyl group bonded to yttrium atoms and arsenate played (Nus) a major role for As(V) uptake on the membrane.

## Acknowledgments

Y.Y appreciates the National University of Singapore for providing the President's Graduate Fellowship during his Ph.D study. C. W. acknowledges the Graduate School for Integrative Sciences and Engineering of the Nus for the Ph.D scholarship. This research/project was partially supported by the National Research Foundation, Prime Minister's Office, Singapore under its Campus for Research Excellence and Technological Enterprise (CREATE) program.

## Appendix A. Supplementary material

Supplementary data associated with this article can be found, in the online version, at <https://doi.org/10.1016/j.jcis.2018.06.003>.

## References

- [1] R. Singh, S. Singh, P. Parihar, V.P. Singh, S.M. Prasad, Arsenic contamination, consequences and remediation techniques: a review, *Ecotoxicol. Environ. Saf.* 112 (2015) 247–270.
- [2] B. Chen, Z. Zhu, Y. Guo, Y. Qiu, J. Zhao, Facile synthesis of mesoporous Ce-Fe bimetal oxide and its enhanced adsorption of arsenate from aqueous solutions, *J. Colloid Interface Sci.* 398 (2013) 142–151.
- [3] C. Wang, X. Liu, J.P. Chen, K. Li, Superior removal of arsenic from water with zirconium metal-organic framework UiO-66, *Sci. Rep.* 5 (2015) 16613.
- [4] C. Wang, M. Lee, X. Liu, B. Wang, C.J. Paul, K. Li, A metal-organic framework/ $\alpha$ -alumina composite with a novel geometry for enhanced adsorptive separation, *Chem. Commun.* 52 (57) (2016) 8869.
- [5] Y. Yu, L. Yu, M. Sun, J.P. Chen, Facile synthesis of highly active hydrated yttrium oxide towards arsenate adsorption, *J. Colloid Interface Sci.* 474 (2016) 216–222.
- [6] Y.M. Zheng, S.F. Lim, J.P. Chen, Preparation and characterization of zirconium-based magnetic sorbent for arsenate removal, *J. Colloid Interface Sci.* 338 (1) (2009) 22–29.
- [7] S.R. Kanel, J.-M. Greneche, H. Choi, Arsenic (V) removal from groundwater using nano scale zero-valent iron as a colloidal reactive barrier material, *Environ. Sci. Technol.* 40 (6) (2006) 2045–2050.
- [8] J. Mayo, C. Yavuz, S. Yean, L. Cong, H. Shipley, W. Yu, J. Falkner, A. Kan, M. Tomson, V. Colvin, The effect of nanocrystalline magnetite size on arsenic removal, *Sci. Technol. Adv. Mater.* 8 (1–2) (2007) 71.
- [9] L. Ma, S. Tu, Removal of arsenic from aqueous solution by two types of nano TiO<sub>2</sub> crystals, *Environ. Chem. Lett.* 9 (4) (2011) 465–472.
- [10] Y. Ma, Y.M. Zheng, J.P. Chen, A zirconium based nanoparticle for significantly enhanced adsorption of arsenate: synthesis, characterization and performance, *J. Colloid Interface Sci.* 354 (2) (2011) 785–792.
- [11] L. Yu, Y. Ma, C.N. Ong, J. Xie, Y. Liu, Rapid adsorption removal of arsenate by hydrous cerium oxide-graphene composite, *RSC Adv.* 5 (80) (2015) 64983–64990.
- [12] D. Zhao, Y. Yu, J.P. Chen, Fabrication and testing of zirconium-based nanoparticle-doped activated carbon fiber for enhanced arsenic removal in water, *RSC Adv.* 6 (32) (2016) 27020–27030.
- [13] J. He, T. Matsuura, J.P. Chen, A novel Zr-based nanoparticle-embedded PSF blend hollow fiber membrane for treatment of arsenate contaminated water: material development, adsorption and filtration studies, and characterization, *J. Membr. Sci.* 452 (2014) 433–445.
- [14] Y.M. Zheng, S.W. Zou, K.G.N. Nanayakkara, T. Matsuura, J.P. Chen, Adsorptive removal of arsenic from aqueous solution by a PVDF/zirconia blend flat sheet membrane, *J. Membr. Sci.* 374 (1) (2011) 1–11.
- [15] A. Razmjou, J. Mansouri, V. Chen, The effects of mechanical and chemical modification of TiO<sub>2</sub> nanoparticles on the surface chemistry, structure and fouling performance of PES ultrafiltration membranes, *J. Membr. Sci.* 378 (1–2) (2011) 73–84.
- [16] A.S. Rocha, A.M. da S. Forrester, E.R. Lachter, E.F. Sousa-Aguiar, A.C. Faro, Niobia-modified aluminas prepared by impregnation with niobium peroxo complexes for dimethyl ether production, *Catalysis Today* 192(1) (2012) 104–111.
- [17] C.J.J. Kuo, G.L. Amy, C.W. Bryant, Factors affecting coagulation with aluminum sulfate-I. Particle formation and growth, *Water Res.* 22 (7) (1988) 853–862.
- [18] J.F. Watts, J. Wolstenholme, An Introduction to Surface Analysis by XPS and AES, 2003, pp. 224.
- [19] R. Boom, I. Wienk, T. Van den Boomgaard, C. Smolders, Microstructures in phase inversion membranes. Part 2. The role of a polymeric additive, *J. Membr. Sci.* 73 (2) (1992) 277–292.
- [20] B. Chakrabarty, A. Ghoshal, M. Purkait, Preparation, characterization and performance studies of polysulfone membranes using PVP as an additive, *J. Membr. Sci.* 315 (1) (2008) 36–47.
- [21] S. Wongchitphimon, R. Wang, R. Jiratananon, L. Shi, C.H. Loh, Effect of polyethylene glycol (PEG) as an additive on the fabrication of polyvinylidene fluoride-co-hexafluoropropylene (PVDF-HFP) asymmetric microporous hollow fiber membranes, *J. Membr. Sci.* 369 (1) (2011) 329–338.
- [22] C. Mbareck, Q.T. Nguyen, O.T. Alaoui, D. Barillier, Elaboration, characterization and application of polysulfone and polyacrylic acid blends as ultrafiltration membranes for removal of some heavy metals from water, *J. Hazard. Mater.* 171 (1) (2009) 93–101.
- [23] R. Srinivasan, R. Yogamalar, A.C. Bose, Structural and optical studies of yttrium oxide nanoparticles synthesized by co-precipitation method, *Mater. Res. Bull.* 45 (9) (2010) 1165–1170.
- [24] H. Liu, S. Deng, Z. Li, G. Yu, J. Huang, Preparation of Al-Ce hybrid adsorbent and its application for defluoridation of drinking water, *J. Hazard. Mater.* 179 (1) (2010) 424–430.
- [25] Y.S. Ho, Adsorption of Heavy Metals from Waste Streams by Peat, University of Birmingham, 1995.
- [26] Y.S. Ho, G. McKay, Pseudo-second order model for sorption processes, *Process Biochem.* 34 (5) (1999) 451–465.
- [27] H. Zeng, M. Arashiro, D.E. Giammar, Effects of water chemistry and flow rate on arsenate removal by adsorption to an iron oxide-based sorbent, *Water Res.* 42 (18) (2008) 4629–4636.
- [28] W.J. Weber, J.C. Morris, Kinetics of adsorption on carbon from solution, *J. Sanitary Eng. Divis.* 89 (2) (1963) 31–60.
- [29] Y.T. Wei, Y.M. Zheng, J.P. Chen, Enhanced adsorption of arsenate onto a natural polymer-based sorbent by surface atom transfer radical polymerization, *J. Colloid Interface Sci.* 356 (1) (2011) 234–239.
- [30] Y. Masue, R.H. Loepfert, T.A. Kramer, Arsenate and arsenite adsorption and desorption behavior on coprecipitated aluminum: iron hydroxides, *Environ. Sci. Technol.* 41 (3) (2007) 837–842.
- [31] D. Zhao, Y. Yu, C. Wang, J.P. Chen, Zirconium/PVA modified flat-sheet PVDF membrane as a cost-effective adsorptive and filtration material: a case study on decontamination of organic arsenic in aqueous solutions, *J. Colloid Interface Sci.* 477 (2016) 191–200.
- [32] T. Li, Z. Zhu, D. Wang, C. Yao, H. Tang, Characterization of floc size, strength and structure under various coagulation mechanisms, *Powder Technol.* 168 (2) (2006) 104–110.
- [33] N. Mameri, A. Yeddou, H. Lounici, D. Belhocine, H. Grib, B. Bariou, Defluoridation of septentrional Sahara water of North Africa by electrocoagulation process using bipolar aluminium electrodes, *Water Res.* 32 (5) (1998) 1604–1612.
- [34] J. He, J.P. Chen, A zirconium-based nanoparticle: essential factors for sustainable application in treatment of fluoride containing water, *J. Colloid Interface Sci.* 416 (416) (2014) 227–234.
- [35] E.M. Vrijenhoek, J.J. Waypa, Arsenic removal from drinking water by a “loose” nanofiltration membrane, *Desalination* 130 (3) (2000) 265–277.
- [36] S. Zhang, X.Y. Li, J.P. Chen, An XPS study for mechanisms of arsenate adsorption onto a magnetite-doped activated carbon fiber, *J. Colloid Interface Sci.* 343 (1) (2010) 232–238.